Hindawi
Advances in Materials Science and Engineering
Volume 2018, Article ID 1069181, 11 pages
https://doi.org/10.1155/2018/1069181

Research Article

Calibration of Material Models against TSTM Test for Crack Risk Assessment of Early-Age Concrete Containing Fly Ash

G. M. Ji,[1] **T. Kanstad**,[2] **and Ø. Bjøntegaard**[3]

[1]*SINTEF Ocean, 7450 Trondheim, Norway*
[2]*The Norwegian University of Science and Technology (NTNU), 7491 Trondheim, Norway*
[3]*Tunnel and Concrete Section, Norwegian Public Roads Administration, Oslo, Norway*

Correspondence should be addressed to G. M. Ji; guomin.ji@sintef.no

Received 16 November 2017; Accepted 18 March 2018; Published 9 May 2018

Academic Editor: Michele Zappalorto

Making reliable cracking risk assessment involves experimental testing and advanced modeling of the time- and temperature-dependent behavior of the properties, the restraint conditions of the structure, and the external environmental conditions. Mineral additives such as silica fume (SF), blast furnace slag (BFS), and fly ash (FA) have been used extensively in production of high performance concrete in the last decades. The mineral additives such as fly ash and blast furnace slag will reduce the hydration heat during the hardening phase, and the mineral additives also have significant influence on the development of mechanic and viscoelastic properties at early age. Within the NOR-CRACK project, extensive test programs were performed to investigate the material properties related to cracking risk of early-age concrete containing mineral additives. In current paper, the advanced modeling of the heat of hydration, volume changes (autogenous shrinkage and thermal dilation) during hardening, the development of mechanical properties (E-modulus, compressive strength, and tensile strength), and creep/relaxation properties are discussed. Tests were performed in "temperature stress testing machine" (TSTM) to measure the restraint stress, and well-documented material models were verified by performing 1-D analysis of restraint stress development in the TSTM (Ji, 2008).

1. Introduction

Cracking of concrete structures may compromise not only structural integrity but also durability and long-term service life. High performance concretes, with low water/binder ratios, are experienced prone to early-age cracking. The main reason is that the high volume changes due to autogenous shrinkage (caused by chemical shrinkage and subsequent self-desiccation) and thermal dilation (caused by hydration heat) lead to significant stresses in conditions of high external restraint.

Early-age cracking has been the subject of extensive research. In recent years, more realistic insights have been gained through various research efforts in related fields, for example, on thermal cracking of early-age concrete by a RILEM technical committee (TC 195-DTD) [1]. Furthermore, the growing number of applications of high performance concrete and the use of massive concrete structures generate a need for a comprehensive methodology to limit/prevent early-age cracking of concrete. The following material properties are main factors which influence the sensitivity of concrete to cracking at early age and which therefore are required for a full evaluation of cracking risk in hardening concrete structures:

(i) The temperature sensitivity (activation energy)
(ii) Heat of hydration
(iii) Coefficient of thermal expansion (CTE)
(iv) Autogenous shrinkage (AS)
(v) Mechanical properties (E-modulus, compressive strength, and tensile strength)
(vi) Creep/relaxation properties

The influences of fly ash on abovementioned early-age concrete properties are investigated in the present study.

Today, there exist several commercially available computer programs capable of calculating the temperature and stress development in hardening concrete structure. Within the past IPACS project [2], a Round Robin calculation was

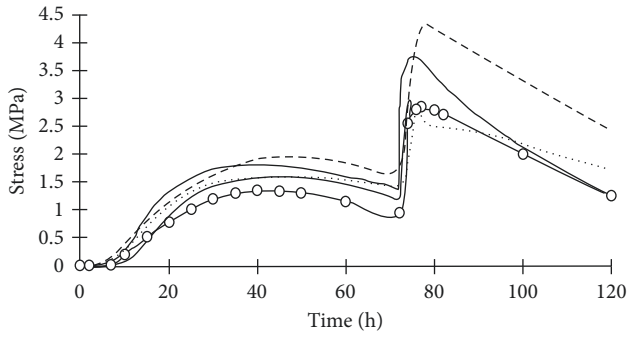

Figure 1: Stress development in hardening concrete slab calculated with different programs [17].

performed, and five different programs were used to simulate temperature and stress development in two examples of hardening concrete structure, and the results are shown in Figure 1 [3]. All calculations were based on same set of laboratory test results describing specific concrete properties. The deviation between the results obtained by different programs may be explained by differences in material modeling, modeling of geometry, and restraint conditions. The deviations were considerable even in the case of stress simulation of hardening specimen in the "temperature stress testing machine" (TSTM) [4] with well-defined temperature and restraining conditions; that is, the material modeling was the only reason for disagreement. The different material models were calibrated to the same experimental data, but in simulation of total behavior of a structure, they gave different results. The comparison gave rise to several questions. What kind of tests is most appropriate for characterization of different material properties? Although different material models are able to describe material properties separately, is the combination of the models able to describe the total behavior of hardening concrete structure or do the different material models match with each other? [3, 5].

Within the NOR-CRACK project, extensive test programs were performed to investigate the material properties listed above [6–9]. In the current paper, the material properties of early-age concrete with fly ash and the advanced modeling of those material properties are presented. The TSTM test results are used to verify the proposed material model and their applicability in the prediction of cracking risk of concrete during the hardening phase.

2. Material Properties

2.1. Concrete Composition. The "SV 40" concrete is a typical high strength concrete used in bridges in Norway, and it has a water-binder ratio (w/b) of 0.42 with 5% silica fume (percentage of OPC weight). The "low-heat" concrete has w/b of 0.46 and contains 36% FA of binder weight (60% of OPC weight) in addition to 5% silica fume (percentage of OPC weight). The composition of the two concretes is presented in Table 1 [10].

In the laboratory relevant concrete properties were measured, that is, heat of hydration; coefficient of thermal expansion; autogenous shrinkage; mechanical properties including the development of compressive strength, tensile strength, and modulus of elasticity; and creep properties [7, 11].

2.2. Mechanical Properties. The modified version of CEB-FIP MC 1990 is used to describe the development of the compressive strength, tensile strength, and modulus of elasticity, and t_0 is introduced in the equations to identify the start of significant mechanical properties development [12, 13]:

$$f_c = f_{c28}\left\{\exp\left[s\left(1-\sqrt{\frac{28}{t_{eq}-t_0}}\right)\right]\right\},$$

$$f_t = f_{t28}\left\{\exp\left[s\left(1-\sqrt{\frac{28}{t_{eq}-t_0}}\right)\right]\right\}^{n_t}, \quad (1)$$

$$E_c = E_{c28}\left\{\exp\left[s\left(1-\sqrt{\frac{28}{t_{eq}-t_0}}\right)\right]\right\}^{n_E},$$

where t_{eq} is the equivalent time, t_0 is the concrete age when the stiffness starts to increase from zero, s is a curve fitting parameter which is determined from compressive strength development, while n_t and n_E are the curve fitting parameters dedicated for the development of the tensile strength and the elastic Young's modulus, respectively. The parameters shown in Table 2 are later used in the numerical analysis of a full-scale field test structure [14]. The development of the compressive strength, tensile strength, and modulus of elasticity for SV 40 and low-heat concrete are shown in Figures 2 and 3.

2.3. Thermal Properties. The thermal properties are the thermal conductivity κ, the specific heat capacity c, and the heat of hydration. The hydration heat depends on the chemical composition of the cement—it increases with the C3S and C3A content—and on the fineness of grinding. Mineral admixtures, such as silica fume (SF), blast furnace slag (BFS), and fly ash (FA), have significant influence on the heat of hydration. Increasing percentage of the BFS or FA content reduces the amount of heat of hydration significantly. Thomas and Mukherjee [15] showed that when 50% of ordinary Portland cement (OPC) was replaced by slag, the heat of hydration decreased by 28% and the maximum temperature rise was reduced from 24°C to 16°C.

The heat production is described by the approach based on the hydration degree (equivalent to maturity age) [16]:

$$Q = Q_\infty\left\{\exp\left[-\left(\frac{\tau}{t_{eq}}\right)^\alpha\right]\right\}, \quad (2)$$

where Q_∞, τ, and α are model parameters that can be determined from the adiabatic temperature curve derived from semiadiabatic measurements of the heat of hydration.

The parameters of the activation energy were determined according to the Norwegian code (NS3656). The results from isothermal tests at three temperature levels, 5, 20, and 50°C, were plotted against equivalent time. Then, the activation energy was found by fitting results at a level of 40% of maximum strength.

Table 1: Concrete composition, all values in kg/m^3.

Concrete	OPC	Fly ash	Silica fume	Coarse aggregate (8–16 mm)	Fine aggregate (0–8 mm)	Total water
SV 40	404	—	20	880	910	178
Low heat	233	140	12	879	899	178

Table 2: Mechanical properties of the SV 40 and low-heat concrete.

Concrete	$f_c(28)$ (MPa)	$f_t(28)$ (MPa)	$E_c(28)$ (GPa)	s	n_t	n_E	t_0 (h)
SV 40	65.11	3.86	31,700	0.197	0.722	0.421	8.0
Low heat	41.20	3.20	33,360	0.418	0.561	0.251	10.5

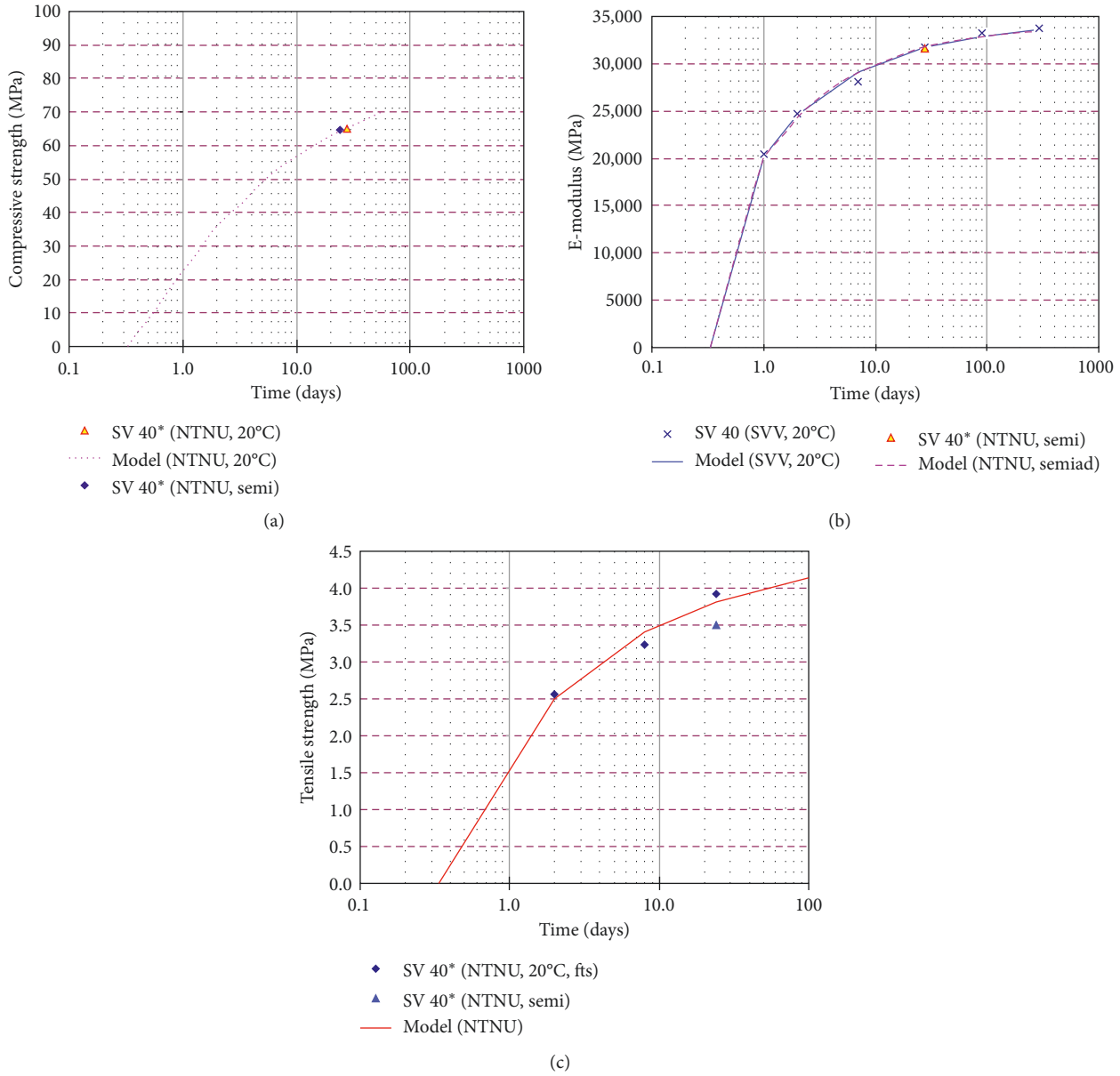

Figure 2: Compressive strength, E-modulus, and tensile strength of SV 40 concrete.

The heat development of the low-heat concrete tested in the laboratory was first used in the analysis, but the calculated maximum temperature was about 10°C lower than the measured maximum temperature. It was later confirmed [18] that, for this particular field experiment, the concrete manufacturer had put fly ash into a silo previously used to store silica fume, but unfortunately, the silo was not completely cleaned, and probably some silica

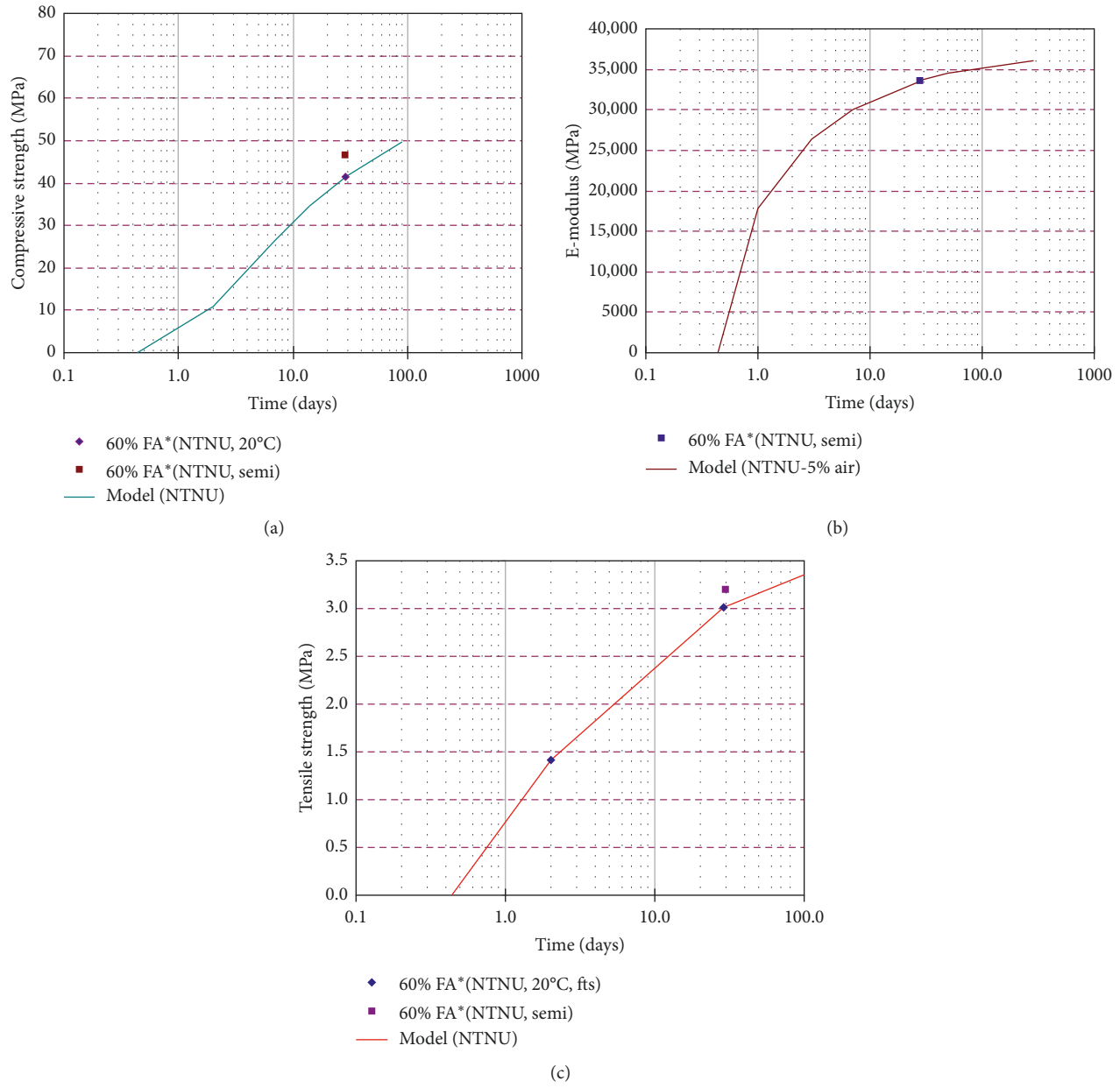

Figure 3: Compressive strength, E-modulus, and tensile strength development of the low-heat concrete.

fume left at the bottom entered the mixture used in this field test. The hydration heat development of the particular concrete mixture used in the field test is shown in Figure 4. The heat development applied in the thermal and structural analysis was about 35% higher than that of the low-heat concrete tested in the laboratory as shown in Table 3 [18].

2.4. Volume Change (Autogenous Shrinkage and Thermal Dilation). The free deformation was measured in the Dilation Rig with a stepwise realistic temperature history for both concretes in the NTNU laboratory [7]. The maximum temperature for SV 40 and low-heat concrete was 56 and 45°C, respectively, with an initial temperature of 20°C, while the maximum temperature for low-heat concrete was 33°C with the initial temperature of 11°C. The autogenous shrinkage is then separated from the thermal dilation by assuming a constant value for the thermal dilation coefficient. The autogenous shrinkage curves of the SV 40 and low-heat (60% FA) concrete are shown in Figure 5.

2.5. Creep. Compressive creep tests for both concretes were performed at different ages at 20°C under sealed conditions, and the results are shown in Figure 6. The double power law is used to model the creep behavior in the numerical simulations, and the compliance function becomes [19–23]

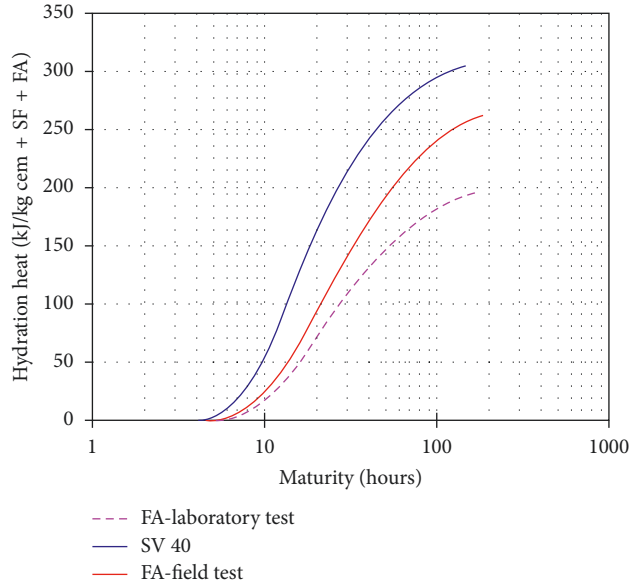

Figure 4: Heat evolutions of SV 40 and low-heat concrete.

Table 3: Thermal properties of SV 40 and low-heat concrete.

Concrete	Q_∞ (kJ/kg cem)	τ	α	Thermal expansion coefficient (10^{-6}/°C)	Arrhenius constant (K)	Thermal conductivity (kJ/°C·ms)	Thermal capacitance (kJ/°C·m^3)
SV 40	319	15.04	1.34	10.54	2645.7	0.0026	2512.2
Low heat (laboratory)	215	17.75	1.20	8.35	4353.1	0.0026	2482.4
Low heat (field test)	290	17.75	1.20	8.35	4353.1	0.0026	2482.4

$$J(t,t') = \frac{1}{E(t_e')}\left(1 + \varphi \cdot (t')^{-d}(t-t')^{p}\right), \quad (3)$$

where t is the concrete age, t' is the concrete age at loading, $E(t_e')$is the E-modulus at the loading age, and φ, d, and p are creep model parameters. In general, two creep tests were performed for each of the loading ages. For the SV 40 concrete, the creep tests were carried out with loading time at 2 and 9 days, respectively, and is shown in Figure 6(a); the model is in good agreement with the experimental results. For the low-heat concrete, the creep tests were carried out at 4 and 7 days, respectively, and it is seen from Figure 6(b) that the estimated the creep strain is slightly lower than the test results. The creep model parameters used in simulation are shown in Table 4.

3. Calibration of the Material Models by the TSTM Test

The systems of the special designed temperature stress test machine (TSTM) as shown in Figure 7 are essentially a closed loop servosystem that can be operated either in load or deformation control mode. The TSTM is described in detail in [4, 7, 24].

The cross section of the specimen is 90 × 100 mm, and the total prismatic length is 1000 mm, and at the both ends, the dimensions are increased in crossheads forming the anchorage. The temperature control system of the TSTM is similar to that of the Dilation Rig. The specimen is sealed with an aluminium plastic foil impermeable to moisture, and drying shrinkage is thus avoided. In the current study, the TSTM is operated in the

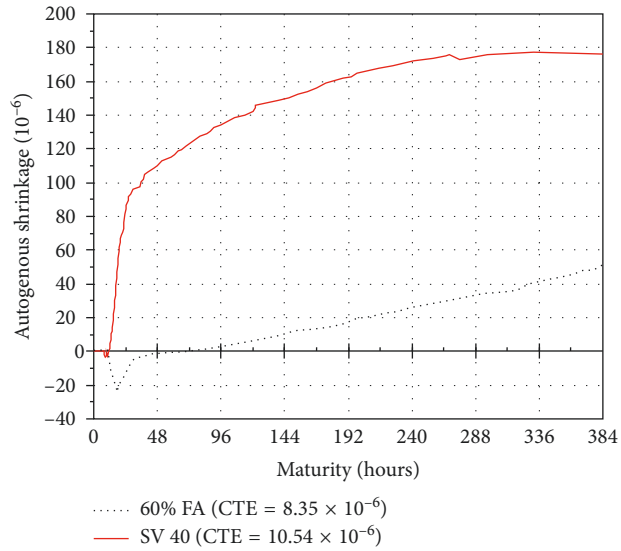

Figure 5: Autogenous shrinkage versus maturity time.

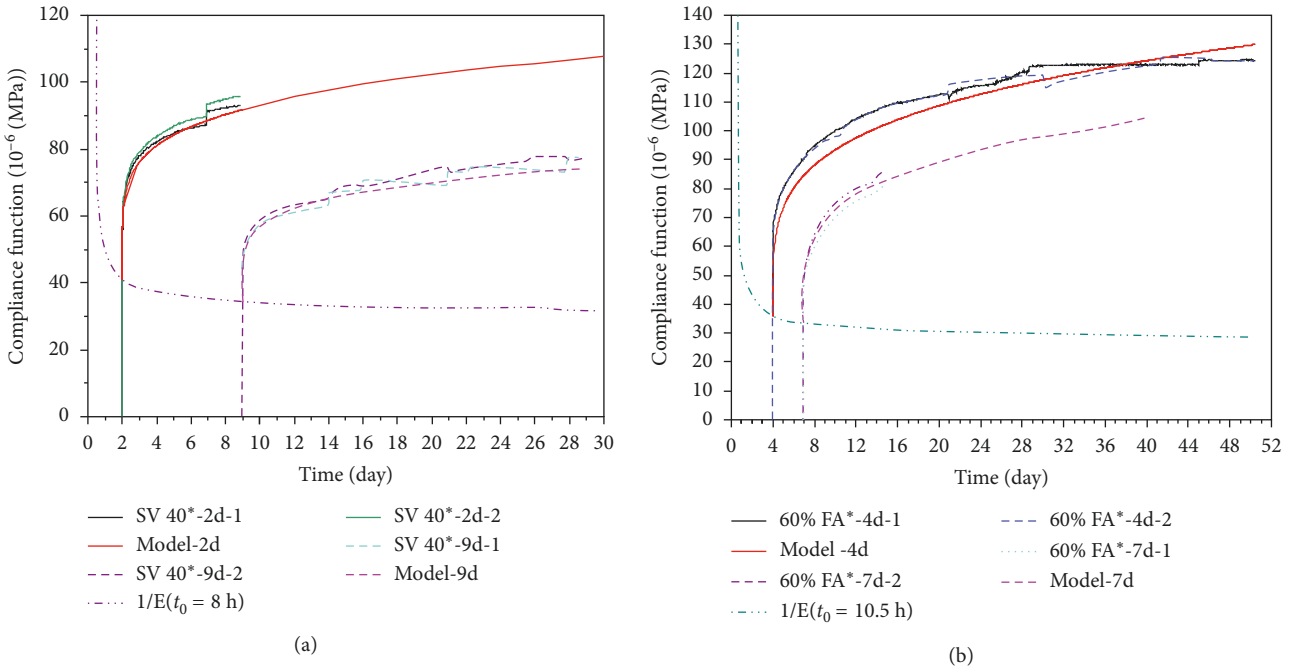

Figure 6: Results of compressive creep tests and double power law. (a) SV 40 concrete. (b) low-heat concrete.

Table 4: Creep parameters for SV 40 and low-heat concrete.

Concrete	d	p	φ
SV 40	0.18	0.18	1.10
Low heat	0.26	0.22	1.60

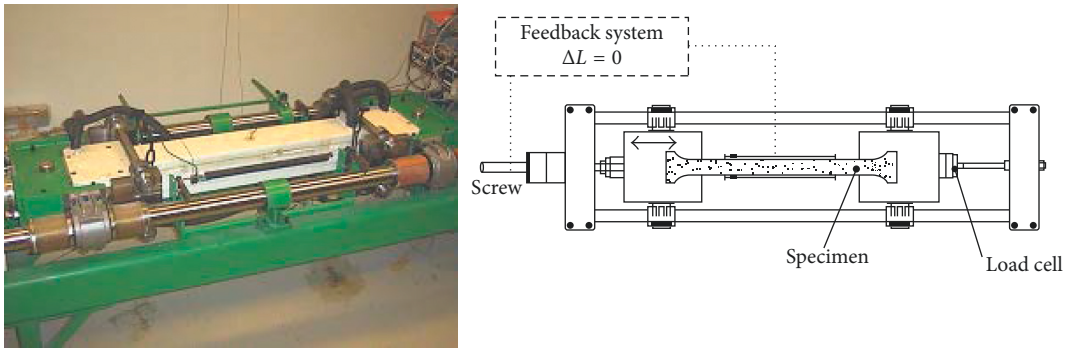

Figure 7: Temperature stress test machine (TSTM).

deformation control mode, and tests were performed under full or partial restraint. The full (100%) restraint condition is provided by an electronic feedback system that moves the left anchoring head of the specimen to compensate for the any length change in the 700 mm midsection of the specimen. A load cell, connected to the right anchoring head, records the restraining force. A partial restraint situation is obtained simply by deactivating the feedback system, meaning that the restraint against deformation is provided by the stiff steel frame of the rig and the anchorage of the specimen. Hence, the restraint degree may vary from test to test, but it is generally around 40%. When partial restraint is used, the deformation of the 700 mm section is recorded as well as the restraining force. The advantage with the partial restraint situation is that an early tensile failure of the specimen is avoided during variable temperature development [7].

The stress development measured in the TSTM is the net effect of all the parameters acting to produce restraint stresses in hardening concrete (ise., thermal dilation, autogenous shrinkage, elastic modulus, and creep/relaxation properties). The TSTM results are used directly for cracking risk comparison of different types of concretes and/or to calibrate the material models by recalculating the restraint stress development in the TSTM.

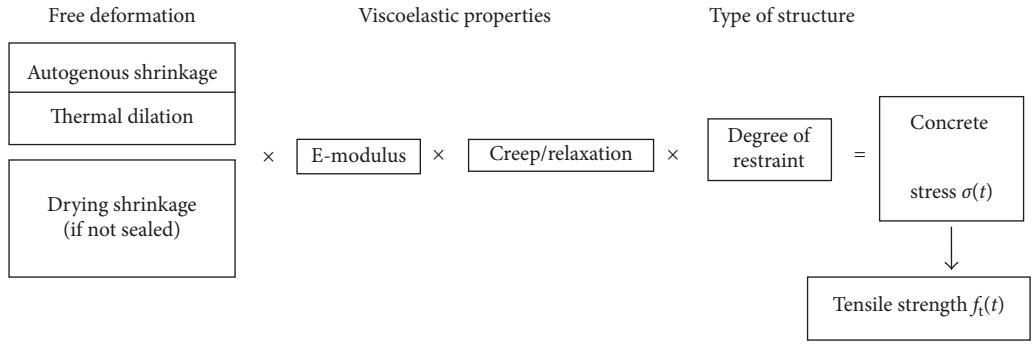

Figure 8: The main factors inducing restraint stress in the TSTM test.

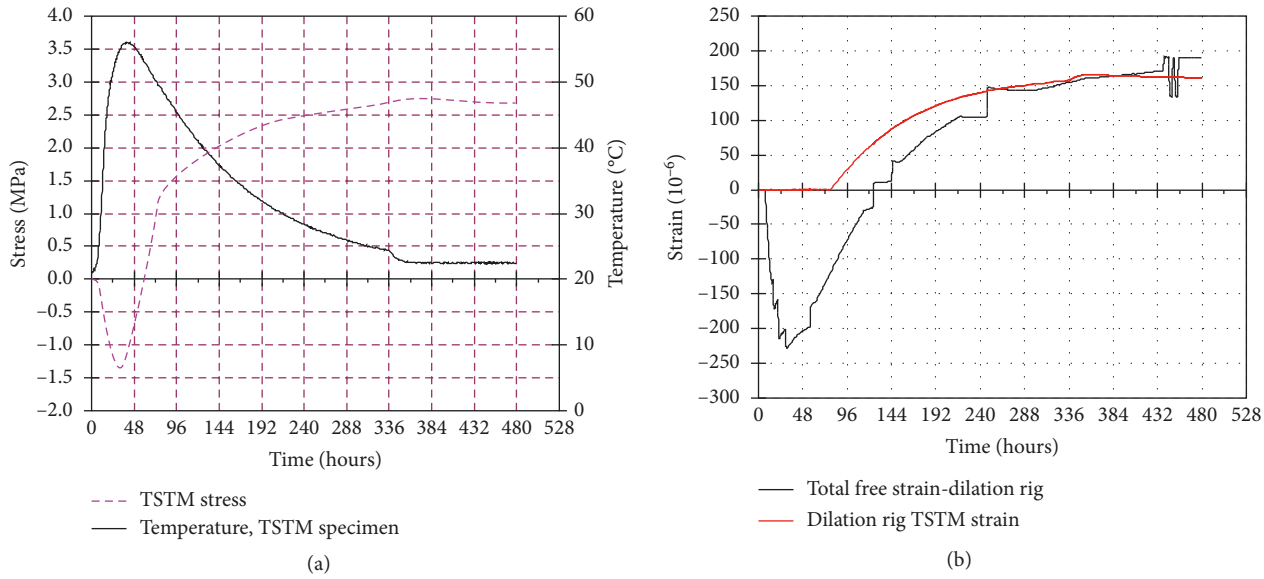

Figure 9: Test results of TSTM and Dilation Rig for SV 40 concrete. (a) Temperature and stress in the TSTM. (b) Deformation in Dilation Rig and TSTM.

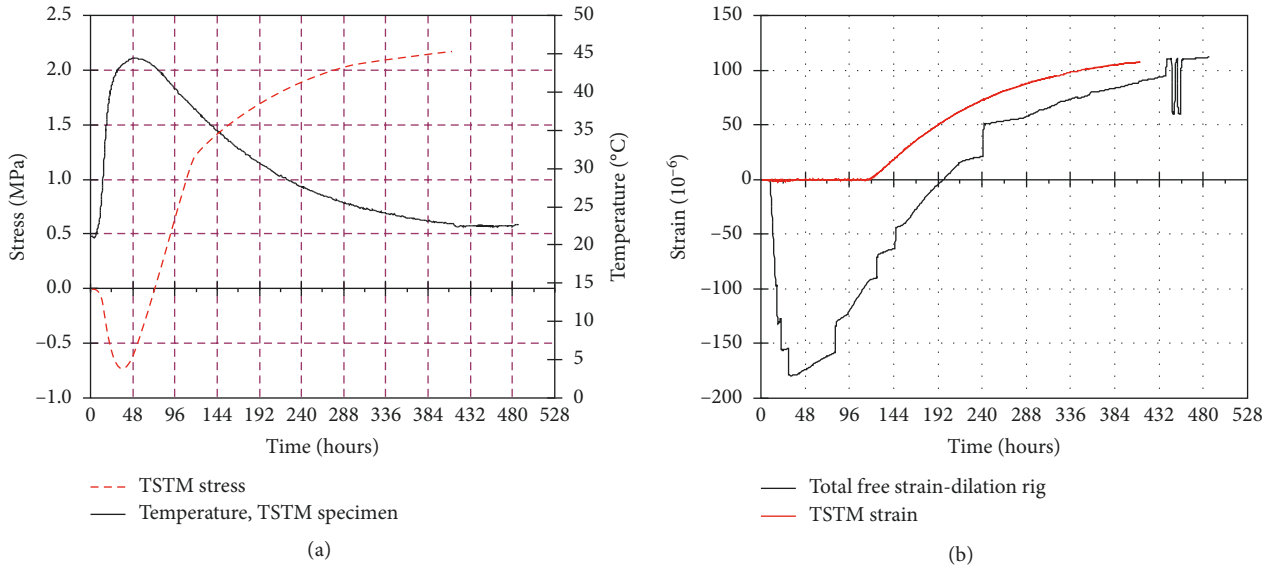

Figure 10: Test results of TSTM and Dilation Rig for low-heat concrete with an initial temperature of 20°C. (a) Temperature and stress in the TSTM. (b) Deformation in Dilation Rig and TSTM.

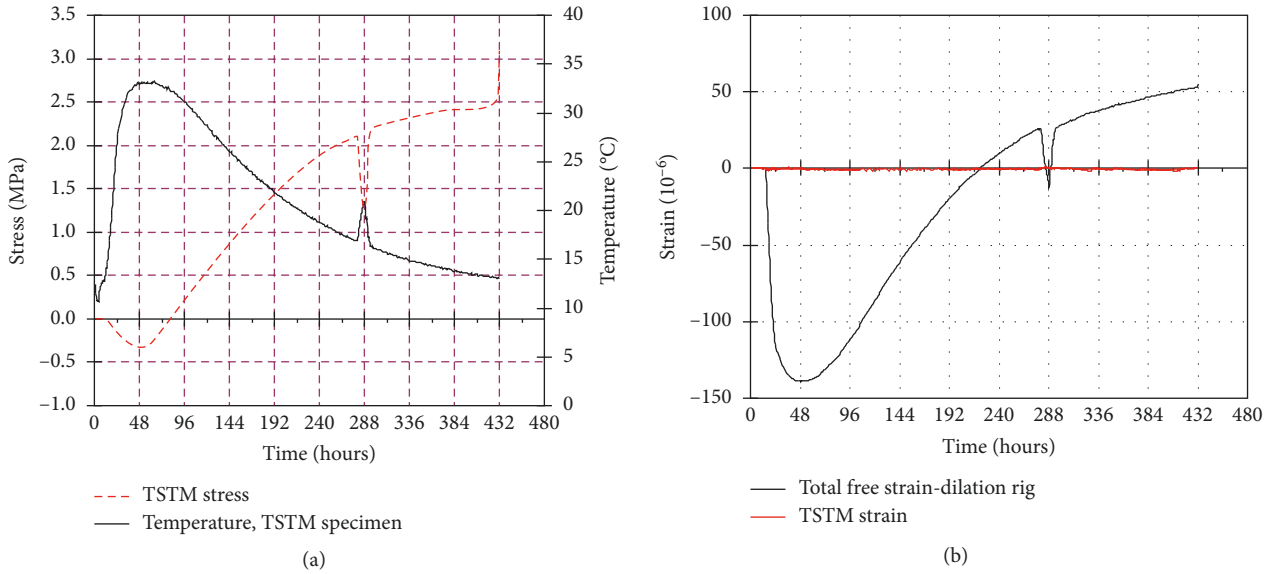

Figure 11: Test results of TSTM and Dilation Rig for low-heat concrete with an initial temperature of 11°C. (a) FA 60% at an initial temperature of 11°C. (b) Deformation in Dilation Rig and TSTM.

In the current study, the tests were performed parallel in the Dilation Rig and TSTM. Thermal dilation and autogenous shrinkage occur simultaneously in the concrete specimens in TSTM and Dilation Rig. The amount of stress generated by thermal dilation and autogenous shrinkage in a given time interval depends on the degree of restraint in TSTM, the elastic modulus, and the creep/relaxation properties of the concrete. Figure 8 illustrates the interplay of these factors in the TSTM test, each of which changes with time.

The integral type of formulation is used in the 1D analysis of restraint stress development in the TSTM:

$$\varepsilon(t) = \int_{t_0}^{t} J(t, t')d\sigma(t') + \varepsilon^0(t). \tag{4}$$

Based on the principle of superposition, the time history is subdivided into time intervals:

$$\varepsilon(t_n) = \sum_{j=1}^{n} J(t_n, t_j) \cdot \Delta\sigma_j + \varepsilon^0(t_n). \tag{5}$$

For continuously varying strain, the second-order algorithm [19], which is based on approximating the integral by the trapezoidal rule, is used to calculate the stress due to a strain increment (or decrement) $\Delta\varepsilon_j$ occurring during the time Δt_j, and a good accuracy can be achieved. The stress increment $\Delta\sigma_j$ is assumed applied in the middle of the jth interval (at time $t_{j-1/2}$). The total loaded induced strain at the end of the jth interval is the sum of the strains due to stress increments $\Delta\sigma_j$, applied during all the previous increments.

$$\varepsilon_{el}(t_j) + \varepsilon_{cr}(t_j) = \sum_{i=1}^{j} J(t_j, t_{i-1/2}) \cdot \Delta\sigma_j, \tag{6}$$

where $t_{i-1/2} = 1/2(t_i - t_{i-1})$.

The constitutive behavior of young concrete in stress rig (TSTM) is defined by the equation as proposed by the CEB-FIP [25]; the strain rate $\Delta\varepsilon_j$ at time t_j may be composed of thermal strain, autogenous strain, creep strain, elastic strain and transient thermal creep strain.

$$\begin{aligned}
\Delta\varepsilon(t_j) &= \Delta\varepsilon_{th}(t_j) + \Delta\varepsilon_{sh}(t_j) + \Delta\varepsilon_{el}(t_j) \\
&\quad + \Delta\varepsilon_{cr}(t_j) + \Delta\varepsilon_{ttc}(t_j), \\
\text{with } \Delta\varepsilon_{el}(t_j) + \Delta\varepsilon_{cr}(t_j) &= \sum_{i=1}^{j} (t_j, t_{i-1/2}) \cdot \Delta\sigma_i \\
&\quad - \sum_{i=1}^{j-1} J(t_{j-1}, t_{i-1/2}) \cdot \Delta\sigma_i, \\
\Delta\varepsilon_{th}(t_j) &= \varepsilon_{th}(t_j) - \varepsilon_{th}(t_{j-1}), \\
\Delta\varepsilon_{sh}(t_j) &= \varepsilon_{sh}(t_j) - \varepsilon_{sh}(t_{j-1}), \\
\Delta\varepsilon_{ttc}(t_j) &= \alpha_T |\Delta T_j| \rho \frac{\sigma(t_j)}{f(t_j)},
\end{aligned} \tag{7}$$

where ε is the measured strain in TSTM, ε_{th} is the thermal dilation, ε_{sh} is the autogenous shrinkage, ε_{el} is the elastic strain, ε_{cr} is the creep strain, and ε_{ttc} is the transient thermal creep strain.

Free deformation measured in Dilation Rig under different temperatures is the sum of ε_{th} and ε_{sh} and is directly used in the stress calculation. Stress increment at time t_j can be determined as

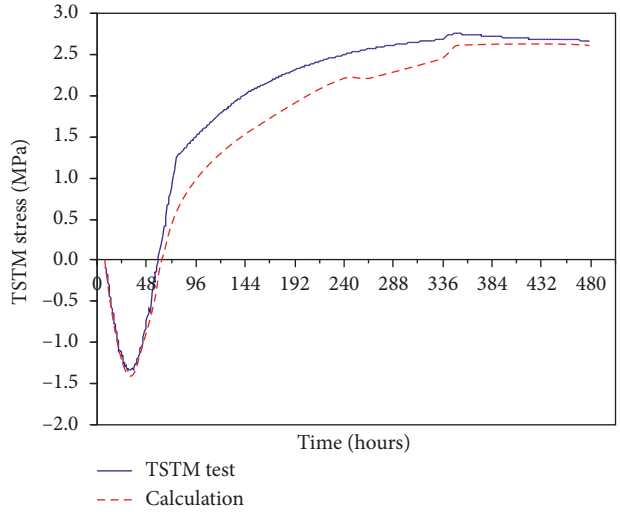

Figure 12: Stress development in the TSTM for SV 40 concrete.

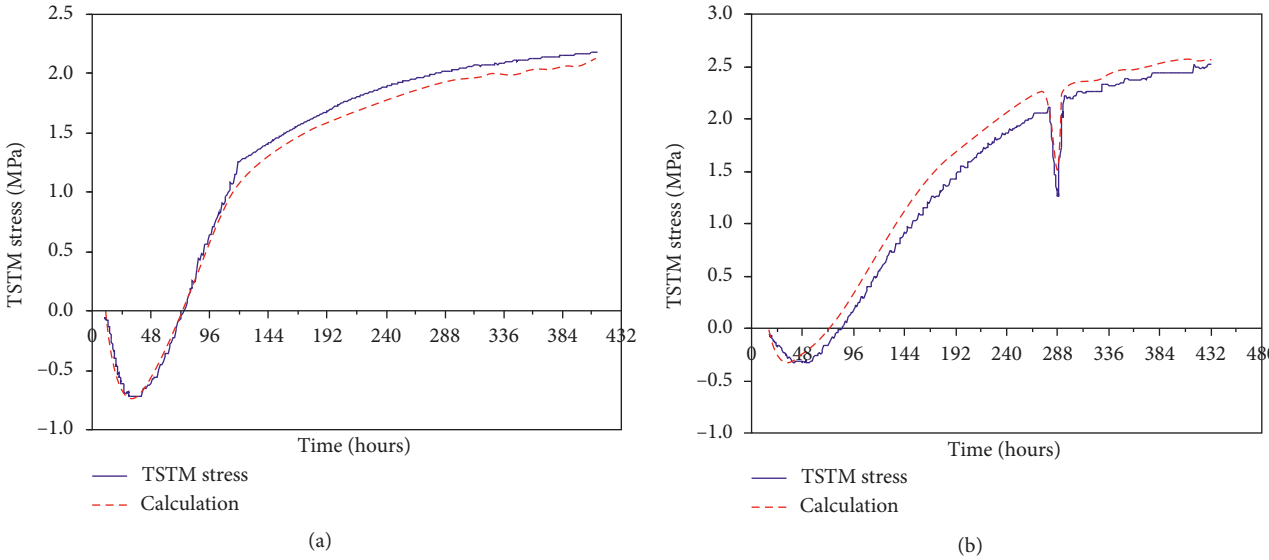

Figure 13: Stress development in the TSTM for low-heat concrete with the initial temperature of (a) 20°C and (b) 11°C.

$$\Delta\sigma_j = \frac{1}{\left(J\left(t_j, t_{j-1/2}\right) + \alpha_T\left|\Delta T_j\right|\rho / f\left(t_j\right)\right)}, \left\{\Delta\varepsilon\left(t_j\right) - \left[\Delta\varepsilon_{th}\left(t_j\right) + \Delta\varepsilon_{sh}\left(t_j\right) + \sum_{i=1}^{j-1}\left(J\left(t_j, t_{i-1/2}\right) - J\left(t_{j-1}, t_{i-1/2}\right)\right)\cdot\Delta\sigma_i + \alpha_T\left|\Delta T_j\right|\rho\frac{\sigma\left(t_{j-1}\right)}{f\left(t_j\right)}\right]\right\}. \quad (8)$$

The imposed temperature histories and measured stress developments in the TSTM for SV 40 and low-heat concrete are shown in Figures 9(a), 10(a), and 11(a), and the strain developments in Dilation Rig and TSTM are shown in Figures 9(b), 10(b), and 11(b). For the SV 40 concrete, the maximum temperature increase is about 36°C from 20°C to 56°C, and the feedback system is deactivated at 76 hours, and the full restraint condition is then changed to the partial restraint condition to prevent break of the specimen during the test. For the low-heat concrete, the TSTM test was first performed at the initial temperature of 20°C, and the maximum temperature rise is 25°C, and the full restraint condition is changed to the partial restraint condition at 120 hours. Another TSTM test was carried out at the initial temperature of 11°C, which represented the approximate air temperature in the field test, under full restraint condition, and the maximum temperature rise is about 22°C.

The comparisons of calculated and measured stress development for SV 40 concrete are shown in Figure 12, and the development of the compressive stress in the first 2 days is in good agreement with the test results, but the development of the tensile stress afterwards is lower than the test

results. The E-modulus of SV 40 concrete at 28 day is relatively low, and it significantly reduces the calculated tensile stress development. The calculated and measured stress developments of the low-heat concrete with 20°C initial temperature are shown in Figure 13(a), and the development of the compressive stress in the first 3 days is in good agreement with the test results, and the development of the tensile stress afterwards is slightly lower than the test results. The stress development of the low-heat concrete with 11°C initial temperature is shown in Figure 13(b), and the development in both compressive and tensile stress is slightly higher than the test results. In general, the material models used in the analysis give a rather good prediction of the stress development in the TSTM test.

4. Conclusion and Discussion

Crack risk assessment of early-age concrete should be based on specific (measured) concrete properties, and the following material properties are main factors which are required for a full evaluation of cracking risk in hardening concrete structures:

(i) The temperature sensitivity (activation energy)

(ii) Heat of hydration

(iii) Volume change: thermal dilation and autogenous shrinkage

(iv) Mechanical properties: E-modulus, compressive strength, and tensile strength

(v) Creep/relaxation properties

It is necessary to perform experimental tests to establish the database for the material properties listed above.

The stress development measured in the TSTM is the net effect of all the parameters acting to produce stresses in hardening concrete (i.e., thermal dilation, autogenous shrinkage, E-modulus, and creep/relaxation properties). TSTM is a suitable tool to investigate the stress development in hardening concrete under realistic temperature conditions and to further optimize the concrete mix to reduce the cracking risk. The measured restraint stress at TSTM is used to verify the material models and its applicability for cracking assessment of early-age concrete. It is recommended to use this procedure to obtain reliable and robust material modeling and to ensure that the combination of the models is able to describe the total behavior of hardening concrete structure.

Conflicts of Interest

The authors declare that they have no conflicts of interest.

Acknowledgments

The financial contribution of the Norwegian Research Council is gratefully acknowledged. The NOR-CRACK partners were the Norwegian University of Science and Technology (project leader), Skanska Norge ASA, Elkem ASA Materials, Norcem AS, Fesil ASA, and the Norwegian Public Roads Administration.

References

[1] R. Springenschmidt, "Thermal cracking in concrete at early ages," *in Proceedings of the International RILEM Symposium,* E&FN Spon, London, UK, 1995.

[2] IPACS, *Brite-Euram Project BRPR-CT97-0437, Improved Production of Advanced Concrete Structures*, 1997.

[3] D. Bosnjak, *Self-Induced Cracking Problems in Hardening Concrete Structure*, Ph.D. thesis, Department of Structural Engineering, NTNU, Trondheim, Norway, ISBN 82-7984-151-2, 2001.

[4] R. Springenschmidt, R. Breitenbucher, and M. Mangold, *Development of the Cracking Frame and Temperature Stress Testing Machine, Thermal Cracking in Concrete at Early-Age,* R. Springenschmidt, Ed., pp. 137–144, E&FN Spon, London, UK, 1994.

[5] A. B. E. Klausen, *Early Age Crack Assessment of Concrete Structures: Experimental Determination of Decisive Parameters*, Ph.D. thesis, NTNU, Trondheim, Norway, ISBN 978-326-7, 2016.

[6] Ø. Bjøntegaard, E. J. Sellevold, and T. Kanstad, "Deformation properties and crack sensitivity in young concrete: experience and guidelines from a 4-year Norwegian R&D project," in *Proceedings of the XIX Nordic Concrete Research Meeting*, Sandefjord, Norway, 2005.

[7] Ø. Bjøntegaard, "Stress development and cracking tendency in hardening concrete: test methods at NTNU," NOR-CRACK Report number A03607, Trondheim, Norway, 2003.

[8] T. Kanstad, T. A. Hammer, Ø. Bjøntegård, and E. J. Sellevold, "Mechanical properties of young concrete: evaluation of test methods for tensile strength and modulus of elasticity determination of model parameters," SINTEF-Report number STF22 A99762, SINTEF, Trondheim, Norway, 1999.

[9] G. M. Ji, *Cracking Risk of Concrete Structures in the Hardening Phase: Experiments, Material Modelling and Finite Element Analysis*, Ph.D. thesis, Department of Structural Engineering, NTNU, Trondheim, Norway, ISBN 978-82-471-1079-9, 2008.

[10] G. M. Ji, T. Kanstad, and Ø. Bjøntegaard, "Analysis of the SVV double wall field test related to the Bjørvika tunnel project," Report number R-7 -04, NTNU, Trondheim, Norway, 2004.

[11] G. M. Ji, Ø. Bjøntegaard, D. Atrushi, T. Kanstad, and E. J. Sellevold, "Compressive and tensile creep of young concrete with mineral additives, creep, shrinkage and durability mechanics of concrete and other quasi-brittle materials," in *Proceedings of the Seventh International Conference*, Nantes, France, 2005.

[12] T. Kanstad, T. A. Hammer, Ø. Bjøntegaard, and E. J. Sellevold, "Mechanical properties of young concrete: part 1: experimental results related to test method and temperature effects," *Materials and Structures*, vol. 36, no. 4, pp. 218–225, 2003.

[13] T. Kanstad, T. A. Hammer, Ø. Bjøntegaard, and E. J. Sellevold, "Mechanical properties of young concrete: part 2: determination of model parameters and test program proposals," *Materials and Structures*, vol. 36, no. 4, pp. 226–230, 2013.

[14] G. M. Ji, T. Kanstad, and Ø. Bjøntegaard, "Numerical modelling of field test for crack risk assessment of early age concrete containing fly ash," *Advances in Materials Science and Engineering*, 2018, In press.

[15] M. D. A. Thomas and P. K. Mukherjee, *The Effect of Slag on Thermal Cracking in Concrete, Thermal Cracking in Concrete at Early Ages*, E&FN Spon, London, UK, ISBN: 0 419 18710 3, 1994.

[16] P. Freiesleben Hansen and J. Pedersen, "Maturity computer for controlled curing and hardening of concrete," *Nordisk Betong*, vol. 1, pp. 19–34, 1977.

[17] J. Olofsson and M. Uhlán, Round Robin Simulation -Ground Slab Examples, Skanska Teknik AB, Stockholm, Sweden, ISBN 91-89580-54-0, 2000.

[18] K. L. Claus and G. M. Ji, "Crack risk modelling of restrained walls—is it possible?—a comparison between measured and computer modelled strains," in *Proceedings of Nordic Seminar*, Trondheim, Norway, 2005.

[19] Z. P. Balant and L. J. Najjar, "Comparison of approximate linear methods for concrete creep," *Journal of the Structural Division*, vol. 99, no. 9, pp. 1851–1874, 1973.

[20] Z. P. Bažant, *Mathematical Modeling of Creep and Shrinkage of Concrete*, John Wiley and Sons, Hoboken, NJ, USA, 1988.

[21] Z. P. Bažant and J. C. Chern, "Concrete creep at variable humidity," *Journal of Engineering Mechanics*, vol. 18, no. 103, 1985.

[22] Z. P. Bažant and J. C. Chern, "Concrete creep at variable humidity: constitutive law and mechanism," *Materials and Structures (RILEM)*, vol. 18, 1985.

[23] A. B. E. Klausen, T. Kanstad, Ø. Bjøntegaard, and E. Sellevold, "Comparison of tensile and compressive creep of fly ash concretes in the hardening phase," *Cement and Concrete Research*, vol. 95, pp. 188–194, 2017.

[24] A. B. E. Klausen, T. Kanstad, and Ø. Bjøntegaard, "Updated temperature-stress testing machine (TSTM): introductory tests, calculations, verification and investigation of variable fly ash content," in *Proceedings of the International Conference: Concreep-10 Mechanisms and Physics of Creep, Shrinkage, and Durability of Concrete and Concrete Structures*, p. 9, Vienna, Austria, ISBN 978-3-9503537-8-5, September 2015.

[25] *CEB-FIP Model Code 90, Design Code, CEB Bulletin No. 213/214*, ISBN: 978-0-7277-1696-5, Thomas Telford, London, 1992.